Photosynthetic electron transport transients in Chlorella vulgaris under fluctuating light

Marlène Bonnanfant, Bruno Jesus, Jeremy Pruvost, Jean-Luc Mouget, Douglas Campbell

Algal Research 44 (2019) 101713

Contents lists available at ScienceDirect

Algal Research

journal homepage: www.elsevier.com/locate/algal

Photosynthetic electron transport transients in *Chlorella vulgaris* under fluctuating light

Marlene Bonnanfant[a,b], Bruno Jesus[c], Jeremy Pruvost[d], Jean-Luc Mouget[a], Douglas A. Campbell[b,*]

[a] Mer-Molécules-Santé (MMS), FR CNRS 3473 IUML, Le Mans Université, Le Mans Cedex 9, France
[b] Department of Biology, Mount Allison University, Sackville, NB, E4L3M7, Canada
[c] Université de Nantes, Faculté des Sciences, Mer-Molécules-Santé (MMS), EA2160, Nantes, France
[d] Université de Nantes, Oniris, CNRS, GEPEA, UMR 6144, F-44600, Saint-Nazaire, France

ARTICLE INFO

Keywords:
Chlorella vulgaris
Solar cultures
Light effect
Chlorophyll *a* fluorescence
Electron Transport Rate

ABSTRACT

Chlorella sp. is both an important model for green algal photosynthesis and is produced using industrial scale photobioreactors. In photobioreactors, cells travel through steep gradients of illumination at rates determined by photobioreactor design, mixing rates, culture density and surface irradiance levels. We used non-invasive, rapid fluorescence measures to show that *Chlorella vulgaris* tolerates short-term exposures to super-saturating irradiance by transiently accelerating electron transport away from Photosystem II. This capacity lasts for only 10–20 s, and longer exposures to supersaturating irradiance induced down-regulation of electron transport through slowing of down-stream electron sinks, induction of non-photochemical quenching and net Photosystem II photoinactivation. Cells previously acclimated to high growth light were able to partially recover from the down regulation within 300–600 s, but cells previously acclimated to low growth light suffered more sustained down-regulation after exposure to super-saturating light. These metrics can be used to guide and constrain culture density, mixing rate and irradiance regime decisions in photobioreactors.

1. Introduction

1.1. Photo-bioreactors and light environments

Light conversion is a key aspect in the optimisation of microalgal cultures. For large scale applications, mass photoautotrophic production is necessary, usually in open ponds or in closed photobioreactors (PBR). Growth rate in these cultivation methods is limited by light, which most of the time, for mass cultures, is obtained from the sun [1]. In such solar cultures, cells experience light fluctuation dynamics across different time scales. Firstly, light fluctuations are driven on an hourly scale by diurnal cycles as sunlight at the surface of the photobioreactor, the photon flux density (PFD), changes during the day. These diel variations shift predictably with season and latitude [2]. Secondly, PFD is also impacted by weather and can be obstructed by clouds for less than minutes to hours [3]. Furthermore, some fast light variations result from cell displacement due to mixing through the strong light gradient in dense cultures which steeply attenuate light with depth. In a few seconds, light can vary from near-dark to super-saturating level [4]. Depending on the light and dark periods, these mixing cycles can lead to a better growth or can have a negative impact compared to continuous light [5–8]. Finally, most microalgae culture systems include cell transits through unlit regions including pumps. Those designed dark fractions can represent more than 20 % of the nominally illuminated volume of the PBR, with residence times from seconds to several minutes. The impact of these dark regions can be quantitatively compared to the impact of L/D cycles [9].

1.2. Time dependencies in photosynthesis processes and mechanisms

Upon light exposure, photons are absorbed by light harvesting complexes [10] which form an effective absorption cross-section serving Photosystem II (σ_{PSII}) or Photosystem I (σ_{PSI}). In PSII, photon energy is transmitted to the reaction centre chlorophyll *a*-protein that contains the primary electron donor P680. P680 is oxidised and an electron is transferred via pheophytin to the quinone acceptor quinone acceptor Q_A and then to the plastoquinone acceptor Q_B within 200 μs [4].

Four such photochemical electron transfers result in a water molecule oxidized, with an O_2 and 4 protons released. These electrons from

* Corresponding author at: Mount Allison University, 63B York St. Sackville, NB, E4L 3G7, Canada.
E-mail address: dcampbel@mta.ca (D.A. Campbell).

https://doi.org/10.1016/j.algal.2019.101713
Received 29 April 2019; Received in revised form 25 October 2019; Accepted 28 October 2019
Available online 11 November 2019

water are used to reduce the oxidized form of P680 within 1 μs. Reduced Q_B joins the plastoquinone pool (PQ pool) and becomes a plastoquinol PQH_2. PQH_2 is re-oxidised by cytochrome b6-f within a life time, termed τ, between 2 and 15 ms [11]. Then, electrons pass through Photosystem I to carbon fixation or to other sinks, notably back to oxygen [12].

Under high light some mechanisms pre-empt saturation of downstream electron transporters. For example there is an electron cycle around PSII, when the oxidized PQ pool decreases, through which about 15 % of the Q_A^- can be directly re-oxidized, without oxidising water [13]. The water to water cycle is another alternative electron cycle (AEC) in which dioxygen (O_2) is photoreduced, via PSI, by the electrons originating from PSII, to re-form water, so that excess photons and electrons are dissipated. This path does not generate net reductant but may contribute to generating trans-membrane electrochemical gradient of protons [14,15]. Green microalgae are also able to modulate the allocation of excitation energy between PSII and PSI. This process, termed a state transition, operates over 5 to 20 min [16,17]. Beyond these mechanisms of photoprotection, Non Photochemical Quenching (NPQ) is probably the most important process that protects cells from excess light. In this regulated process, excess light energy which cannot be used for photosynthesis, is dissipated as heat. This process is induced in a timescale of seconds to a few minutes [18]. However, when cells are exposed to a change in the irradiance level for a longer time, they change their pigment content through processes of photoacclimation over generational timescales [19]. Finally, if the light energy capture outruns protective processes, then PSII photochemical damage can in turn outrun counteracting repair processes, leading to net photoinhibition. Nevertheless, in many taxa, rapid turnover of PSII protein subunits mediates PSII repair after photoinactivation [20,21].

1.3. σ_{PSII}' and $1/\tau'$ determine achieved Photosystem II electron transport

Chlorophyll fluorescence is an information rich, rapid and non-invasive approach to monitoring photosynthetic performance and acclimation state. Chlorophyll fluorescence-based estimators of PSII electron transport are founded upon incident irradiance (I), $\mathbf{\sigma_{PSII}'}$, a parameter for the capture and delivery of excitation to PSII, and a counteracting parameter, $\mathbf{1/\tau'}$, for the capacity to carry electrons away from the excited PSII [22]. Both functional parameters show a genomically-determined range of short-term regulatory and longer-term acclimatory responses to the environment.

σ_{PSII} can be extracted from a fit of fluorescence rise from F_0 towards F_M in response to cumulative incident photons m^{-2} [23], applied by a train of flashlets in the widely used **F**ast **R**epetition & **R**elaxation **f**luorescence (FRRf) protocol [23]. Under illumination σ_{PSII}' can be down- or up-regulated through photoprotection mechanisms from levels observed in darkness [24]. Induction of regulatory responses to increasing light can provoke down-regulation of σ_{PSII}', with evidence for thresholds for the progressive induction of NPQ down regulation, in response to the degree of closure of the PSII pool, to the length of time held above an induction threshold, and/or the influence of photoreceptor mediated signalling [15,25].

Once a PSII is closed by excitation delivered through σ_{PSII}, $1/\tau'$ acts to re-open PSII for further photochemistry. Note that $1/\tau'$ is estimated as a rate constant for re-opening of PSII after a single turnover saturating flash, which, because of AEC, does not imply that all the electrons leaving PSII are directed towards assimilatory biosynthesis. A variable fraction of photochemical electrons, dependent upon time and growth rate, is indeed retained in biomass [26–28]. Upon illumination $1/\tau'$ can accelerate or decelerate [29] depending upon physiological state and the illumination level. σ_{PSII}' and $1/\tau'$ show both short and longer term responses to changing irradiance [24,29,30], so that the resultant rate of electron transport through PSII, termed PSII ETR, observed at a given irradiance can vary and may show hysteresis [31] depending upon the short- and longer-term history of the illuminated sample.

1.4. *Chlorella vulgaris* as a model and industrial organism

Chlorella vulgaris is a freshwater green microalgae, first described in 1890 by Beyerinck [32]. This species has been used as a model in many studies [20,33,34] and is also produced on large scales because of its nutritional benefits [35].

Using the model green alga *Chlorella* we used non-sequential light curves [29,31] of different durations to investigate the interactive effects of light and time upon achieved electron transport rates, as mediated through up- and down- regulation of σ_{PSII}' and $1/\tau'$ extracted from FRRf measures. Such non-invasive measures are amenable to rapid, low-cost real time monitoring of bioreactor performance across mixing and irradiance regimes.

2. Material and methods

2.1. Culture protocol

Chlorella vulgaris CCAP 21119 was grown in a modified Bold's Basal Medium at 23 °C under 30 μmol m^{-2} s^{-1} (low light, LL) or 330 μmol m^{-2} s^{-1} (high light, HL). Light in growth chambers was provided by warm white T8 fluorescent tubes and measured with a microspherical quantum sensor (Walz, Effeltrich, Germany). All cultures were grown in 250 mL Erlenmeyer flasks. The photoperiod started at 07:00 and stopped at 19:00 giving 12:12 L:D cycle. To track growth, chlorophyll fluorescence was measured at 680 nm with an excitation at 440 nm before and after dilutions in new fresh medium. Growth rate was estimated on the basis of change in chlorophyll fluorescence as:

$$\mu = \frac{ln(N_t) - ln(N_0)}{\Delta t}$$

where N_t is the chlorophyll fluorescence emitted by the culture at time t and N_0 the fluorescence at time 0. Subculturing was every 2–3 days to maintain cells in exponential phase [36].

2.2. Light treatment and Fast Repetition Rate fluorescence measurement

Depending on the culture concentration, dilutions were made into fresh medium prior to optical measurements. 2 mL of each culture were loaded into a 1 cm spectrophotometer cuvette. For each light treatment protocol a parallel sample with + inhibitor was prepared by adding 50 μL of 20 mM dithiothreitol (DTT) into the cuvette to inhibit the xanthophyll cycle [37] that mediates accumulation of much of the NPQ in green algae. For samples for treatments with cumulative light exposures of at least 30 min, a second sample + inhibitor was made by adding 20 μL of 50 g L^{-1} lincomycin [38,39] stock solution in the cuvette to block the PSII repair cycle. Triplicates were made for each condition. The culture was mixed in the cuvette with a stir bar and maintained at 23 (+/− 1) °C. The culture was then dark acclimated for 15 min to allow action of the inhibitor, if any, and relaxation of the growth light acclimation state.

An FL3500 fluorometer Superhead (Photon Systems Instruments, Drasov, Czech Republic) was used to both apply light treatments and to measure the Chl *a* fluorescence using a Fast Repetition Rate fluorescence (FRRf) induction protocol [23,40] following previous works [24,29]. Fig. 1 presents schematic summaries of the measurement (Fig. 1A) and light treatment protocols (Fig. 1B, C and D) we applied to *C. vulgaris*. Fig. 1A shows a representative example of the double FRRf protocol applied at each light step. At the end of each light period (Fig. 1B, C and D) a FRRf induction/relaxation flashlet series ({1.2 μs flashlet + 2 μs darkness} × 40 = 128 μs, at 27527 μmol.m^{-2}.s^{-1} of blue (455 nm) light) was applied on top of the actinic light, if any (Fig. 1A). These FRRf settings were sufficient to drive the samples to saturated maximum F_M level within 30 of 40 consecutive flashlets (Fig. 1A) [41]. After the rapid train of 40 cumulatively saturating flashlets we then applied a further 15 flashlets logarithmically spaced

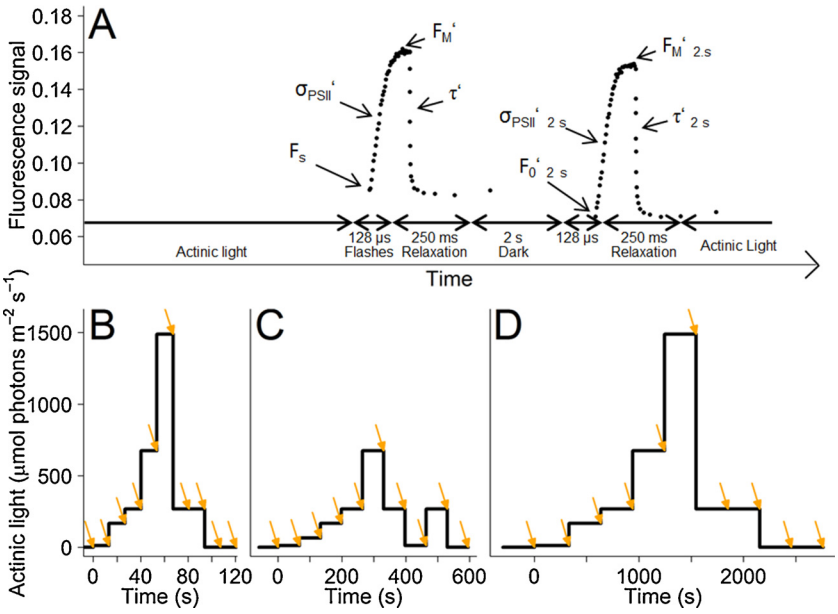

Fig. 1. Fluorescence measurement and light treatment protocols. 1A, FRRf protocol applied at each light step, with an induction/relaxation curve applied on top of actinic light, and then again after 2.5 s of darkness to allow re-opening of PSII.1B, 10 s, 1C, 60 s and 1D, 300 s durations for light exposure periods in treatment protocols. Arrows indicate timing of applications of the FRRf measures during the light treatment protocols.

over 250 ms. This allowed downstream electron transport time to progressively re-open the pool of PSII between each probe flashlet, thereby generating an negative exponential curve. Then a 2 s dark period intervened to allow PSII to fully re-open, and we applied a second FRRf induction/relaxation (Fig. 1A). We applied the protocol in a sequence of actinic light periods, ranging from 0 to 1490 µmol m^{-2} s^{-1}, as shown schematically in Fig. 1B, C and D. The duration of light periods was 10 s (Fig. 1B), 60 s (Fig. 1C) or 300 s (Fig. 1D), depending upon the protocol. Note that the three light treatment protocols plotted here in sequence across the X axes (Fig. 1B, C and D) were actually applied to separate culture samples to limit issues with progressive photoinhibition or acclimation. Nevertheless we chose the 10, 60 and 300 s treatment period durations so that each light treatment trajectory overlapped with the duration of the first steps of the next longest trajectory. Arrows (Fig. 1B, C and D) indicate the timing of applications of the FRRf measures during the light treatment protocols.

2.3. Fluorescence parameters

For each FRR induction and relaxation curve we exported the data from the FluorWin data capture software (Photon Systems Instruments, Drasov, Czech Republic). We used the psifluo package [42] running under the R statistical programming environment [43] to fit the fluorescence rise profile using a model [23] with four parameters:

- minimal fluorescence, F_0, before any closure provoked by the sequence of flashlets;
- maximal fluorescence, F_M, once all PSII are closed by the cumulative action of the sequence of flashlets;
- the effective absorption cross section for PSII photochemistry, σ_{PSII} (A^2 $PSII^{-1}$), which is based upon a target concept whereby incident photons are captured by the pigments serving PSII and thereby drive an increase in fluorescence; and
- the coefficient of excitonic connectivity ρ which measures the departure of the rise profile from a simple exponential function, and which is believed to reflect equilibration of excitation among PSII centres during the sequence of flashlets.

We thereby determined F_0, F_M, σ_{PSII}, ρ after the initial dark period. We then used the same measurement and fitting protocol to determine F_S, F_M', σ_{PSII}' ρ′ for each actinic light period; and $F_0'_{2\ s}$, $F_M'_{2\ s}$, ρ′$_{2\ s}$, $\sigma_{PSII}'_{2\ s}$ following 2 s of darkness immediately after each actinic light period (Fig. 1). We could then estimate variable fluorescence in the illuminated state, F_V', as $F_M'_{2\ s}$ - $F_0'_{2\ s}$. In parallel we used the psifluo package [42] to fit the re-opening curves with a single phase exponential model to estimate an overall lifetime for re-opening of PSII [44], τ, or τ′ if measured immediately after illumination. The reciprocal 1/τ′ is then a rate constant for re-opening of the PSII pool following complete closure.

We estimated the quantum yield for PSII photochemistry under light acclimated conditions but with all PSII opened as:

$$F_V'/F_M'_{2s} = \frac{(F_M'_{2s} - F_0'_{2s})}{F_M'_{2s}}; \quad (1)$$

We estimated the yield [45,46] of photochemical electron transport (YPSII) under actinic illumination as:

$$YPSII = \frac{(F_M' - F_S')}{F_M'}; \quad (2)$$

YPSII is arithmetically equivalent to F_V'/F_M' multiplied by the fraction of PSII remaining open under the given illumination (Eq. (6)).

We estimated the yield of non-photochemical quenching (YNPQ) as:

$$YNPQ = F_S/F_M' - F_S/F_M \quad (3)$$

and the yield of non-regulated excitation dissipation (YNO) as:

$$YNO = F_S/F_M \quad (4)$$

In some cases in phytoplankton the maximum of F_M or F_M' is not found from measures taken in darkness, but rather from measures taken under, or just after, low to moderate light levels. We therefore followed Serôdio et al. [47] and used the maximum value of F_M (F_M') attained for a given sample, not necessarily the value measured after initial dark acclimation, as our basis for estimation of YNPQ and YNO. This avoids confusing values for YNPQ or YNO when plotted vs. a series of light levels.

Electron transport rate was estimated as [48]:

$$\text{PSII ETR (e PSII}^{-1}\,\text{s}^{-1}) = \frac{\sigma_{PSII}}{\frac{F_V}{F_M}} \times \text{YPSII} \times \text{I} \times (6.022 \times 10^{17}\ \text{photons}\,\mu\text{mol}^{-1}) \times (1 \times 10^{-20}\ \text{m}^2\,\text{A}^{-2}) \quad (5)$$

Where I is actinic irradiance (µmol photons m^{-2} s^{-1}).

σ_{PSII} convolutes both the absorption cross section for PSII, and an implicit quantum yield for conversion of absorbed excitation to

photochemistry. In this formulation we use σ_{PSII} measured in darkness, which we divide by our metric of maximum quantum yield measured in darkness, F_V/F_M. This cancels the quantum yield implicit in σ_{PSII}, leaving us with an absorption cross section serving PSII in darkness. We then multiply by YPSII, the quantum yield for photochemistry under illumination, which as discussed above is arithmetically equivalent to the fraction of PSII still open under illumination (Eq. (6)) multiplied by F_V'/F_M'. This apparently overly convoluted equation allows us to use σ_{PSII} and F_V/F_M reliably measured in darkness and YPSII, which can usually be reliably measured even under high actinic light. In contrast, although σ_{PSII}' can be estimated under actinic light the fitting routine for extraction of the parameters can become unreliable for FRRf induction curves obtained under high actinic light.

We estimated the coefficient of photochemical quenching (q_P) as a metric of the fraction of open PSII centres derived from fluorescence levels [49]:

$$q_P = (F_M' - F_S)/(F_M' - F_0')$$
$$q_P = \frac{(F_M' - F_S')}{(F_M' - F_0')}; \quad (6)$$

Alternatively, a model can be used to estimate a conceptually equivalent metric of the fraction of PSII centres, and then PSII ETR [22], solely from parameters derived from the shape of a single fluorescence induction and relaxation profile, thereby avoiding use of absolute fluorescence levels, which can be technically challenging to estimate or compare across samples or instruments.

$$[PSII]_{open} \leftrightarrow [PSII]_{closed} \quad (7)$$

Under some steady state irradiance:

$$[PSII]_{open} \times I \times \sigma_{PSII}' = [PSII]_{closed} \times 1/\tau' \quad (8)$$

where I is the irradiance in photons m^{-2} s^{-1}, σ_{PSII}' has units of m^2 $quanta^{-1}$, and $1/\tau'$ has units of s^{-1}.

Assuming that:

$$[PSII]_{open} + [PSII]_{closed} = [PSII]_{total} \quad (9)$$

We can then re-arrange Eq. (8) to:

$$[PSII]_{open}/[PSII]_{total} = \frac{1}{(1 + (\sigma_{PSII}' \times I \times \tau'))} = [1 - C] \quad (10)$$

where [1-C] is the proportion of open PSII, a metric comparable to the more familiar q_P derived from steady state fluorescence levels (Supp. Fig. 1), and where again I is the irradiance in photons m^{-2} s^{-1}, σ_{PSII}' has units of m^2 $quanta^{-1}$, and $1/\tau'$ has units of s^{-1}.

The rate of electron transport through PSII [22,50,51] can then be estimated as:

$$PSIIETR(ePSII^{-1}s^{-1}) = I \times \sigma_{PSII}' \times [1 - C] \quad (11)$$

Note that all of the parameters for Eq. (11) can be extracted from a single FRRf induction/relaxation profile applied at a given irradiance I, with a total measurement time of ~1–2 s, thereby eliminating any requirement for cross-comparison of metrics taken from different FRRf induction curves under different conditions. In Supp. Fig. 2 we compare the PSII ETR estimates from Eqs. (5) & (11), showing that the equations display differential sensitivity to the presence of inhibitors.

2.4. Data analyses

The following R [43] packages were run under the RStudio [52] environment for data analyses and presentation: psifluo [42], MinPack.lm [53], MASS [54], nlstools [55], ggplot2 [56], tidyverse [57], ggpubr [58], grid [43], gridExtra [59] and shape [60].

3. Results and discussion

3.1. Electron transport rate light responses and hysteresis

Fig. 2 shows PSII ETR (e- $PSII^{-1}$ s^{-1}), estimated using Eq. (5), as a function of instantaneous actinic light level in *C. vulgaris* cultures. Arrows show the direction of increasing time of treatment; dashed lines show steps that follow the maximum applied actinic light, to emphasize hystereses of responses. *C. vulgaris* shows an acceleration of PSII ETR under saturating light after brief (10–20 s) exposure to super-saturating light (Fig. 2A, B). This pattern holds true for cultures from both low light and from high light, although the effect is more marked for the low light cultures (Fig. 2A vs. B). This acceleration is, however, only transient because exposure to 60–120 s of super-saturating light (Fig. 2C, D) leads to a small drop in light-saturated PSII ETR, while more prolonged exposures for 300–600 s lead to a strong inhibition of PSII ETR (Fig. 2E, F). At the level of PSII ETR, *C. vulgaris* can thus exploit transient exposures to inhibitory super-saturating light by accelerating electron transport upon a return to saturating light levels. Longer super-saturating exposures, however, impose a sustained penalty upon return down to saturating light levels. We next sought to understand the mechanism(s) underlying these interactive responses to light and time.

3.2. Changes in YPSII driven by σ_{PSII}' and $1/\tau'$ explain hystereses in PSII ETR responses

The averaged (n = 3) PSII ETR estimates presented in Fig. 2 are based upon Eq. (5). For a given sample exposed to a given trajectory of light periods σ_{PSII} and F_V/F_M are constant inputs to the estimates of PSII ETR. Therefore the dynamics and hystereses seen in Fig. 2 derive from the light and time responses of YPSII within a replicate, compounded by any variations in σ_{PSII} and F_V/F_M among replicates. The patterns of YPSII as a function of instantaneous actinic light level in *C. vulgaris* cultures are illustrated in Fig. 3. Note that YPSII was measured in the presence of actinic illumination. As in Fig. 2 we see a positive hysteresis with a small increase in YPSII after brief (10–20 s) of supersaturating light (Fig. 3A, B). This positive effect disappears with exposures of 60–120 s of supersaturating light (Fig. 3C, D), and reverses to a sustained inhibition of YPSII after 300–600 s exposure to supersaturating light (Fig. 3E, F).

YPSII is in turn an integrative measure of the quantum yield of electron transport through open PSII centres, encompassing both changes in the delivery of excitation to drive PSII photochemistry through $\sigma_{PSII}' \times I$, and changes in the re-opening of PSII after a photochemical event, which is determined by the down-stream capacity to remove photochemically generated electrons from PSII, $1/\tau'$. Therefore changes in YPSII are driven by changes in I (the X axes of Fig. 2), but any hysteresis in the response of YPSII to changing light instead reflects changes in σ_{PSII}', and/or $1/\tau'$, over the course of the light treatment protocol (Fig. 1B, C and D).

Fig. 4 therefore shows $\sigma_{PSII',2\,s}$ as a function of actinic light in *C. vulgaris* cultures. We used the $\sigma_{PSII',2\,s}$ measures taken after 2 s of darkness, to allow re-opening of PSII to support consistently reliable estimates of $\sigma_{PSII',2\,s}$ across the light protocol steps. Our estimates of $\sigma_{PSII'}$ under actinic illumination were in some cases scattered (data not shown) because $\sigma_{PSII'}$ derives from a fit of the change in variable fluorescence (Fig. 1A) and under actinic illumination the amplitude of remaining variable fluorescence can be small. The drawback of this approach is that over the 2 s dark re-opening period some fraction of non-photochemical quenching may also relax, leading to potential discrepancies from estimates of $\sigma_{PSII'}$ taken under actinic light [36]. Induction of non-photochemical quenching mechanisms would be expected to cause a drop in $\sigma_{PSII',2\,s}$ [24]. Instead, across our data we observed either no hystereses in $\sigma_{PSII',2\,s}$ (Fig. 4A, F) or upward shifts in $\sigma_{PSII',2\,s}$ (Fig. 4B,C, D, E) following transient exposures to super-saturating light, particularly in cells from high light growth after 10–120 s

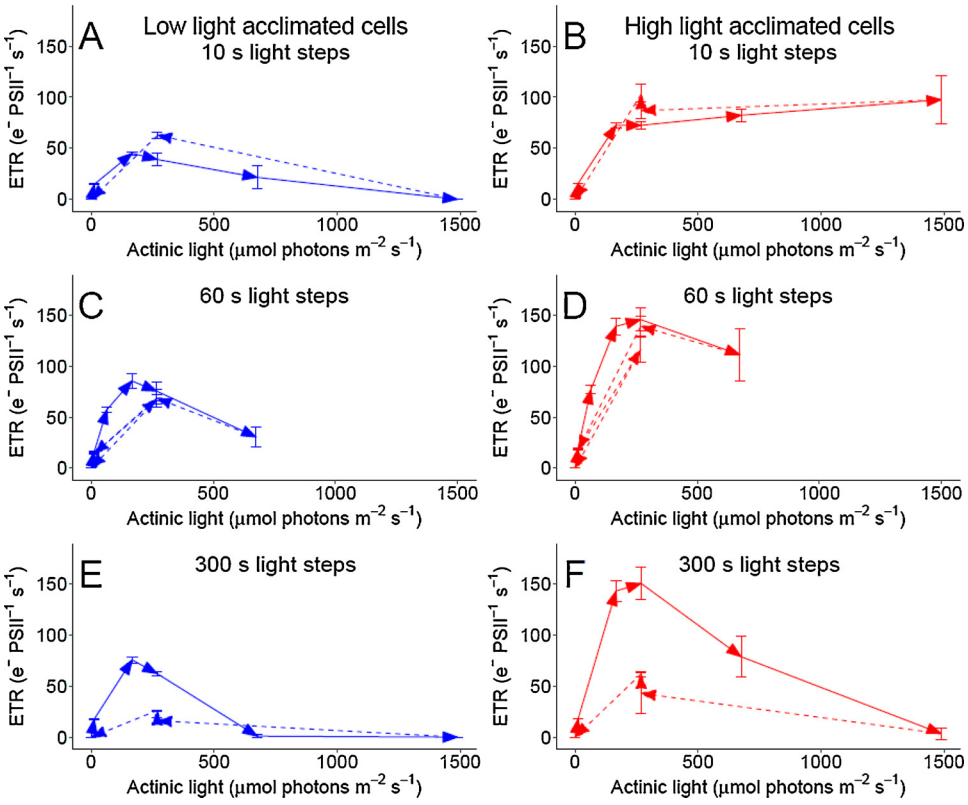

Fig. 2. PSII ETR (e- $PSII^{-1}$ s^{-1}) as a function of instantaneous actinic light level in *C. vulgaris* cultures. Each light period lasted for 10 s (A, B), 60 s (C, D) or 300 s (E, F). Cultures were grown at 30 µmol m^{-2} s^{-1} (low light, A, C, E) or 330 µmol m^{-2} s^{-1} (high light, B, D, F). Arrows show direction of increasing time of treatment; dashed lines show light steps done after the maximum applied actinic light, to emphasize hystereses of response. Error bars represent standard deviation of three replicates. PSII ETR was estimated according to Eqn. 5.

exposure to super-saturating irradiance (Fig. 4B,D). Thus, we found no evidence for down-regulation of $\sigma_{PSII',2\,s}$ in response to transient exposures to super-saturating light up to 600 s duration, and in some cases we observed increases in $\sigma_{PSII',2\,s}$. Increases in $\sigma_{PSII'}$ therefore contribute to some cases of acceleration in PSII ETR in high light cells transiently exposed to super-saturating irradiance (compare Figs. 2B and 4 B) but in the other cases changes in PSII ETR are not explicable by changes in $\sigma_{PSII',2\,s}$ (Compare Figs. 2C, D, E and F with 4 C, D, E and F).

Fig. 5 shows the change in $1/\tau_{',2\,s}$, the rate constant for re-opening of PSII in *C. vulgaris* cultures after 2 s in darkness, as a function of the

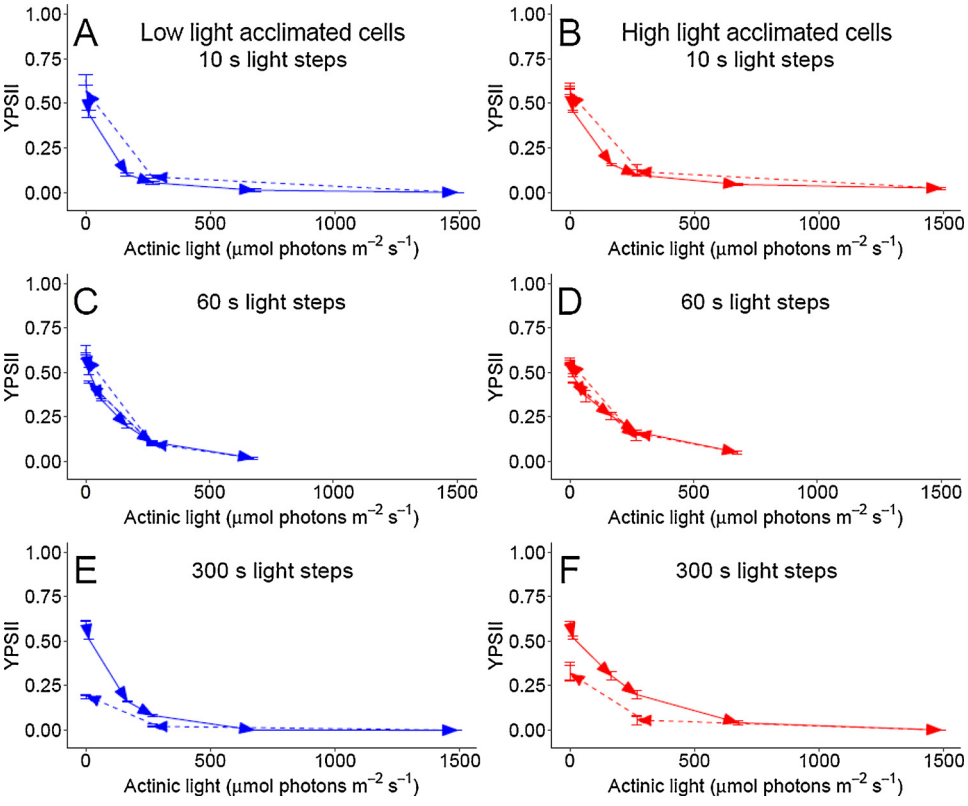

Fig. 3. YPSII quantum yield for PSII electron transport measured under actinic light levels in *C. vulgaris* cultures. Each light period lasted for 10 s (A, B), 60 s (C, D) or 300 s (E, F). Cultures were grown at 30 µmol m^{-2} s^{-1} (low light, A, C, E) or 330 µmol m^{-2} s^{-1} (high light, B,D,F). Arrows show direction of increasing time of treatment. Dashed lines show light steps done after the maximum applied actinic light to emphasize hystereses of response. Error bars represent standard deviation of three replicates.

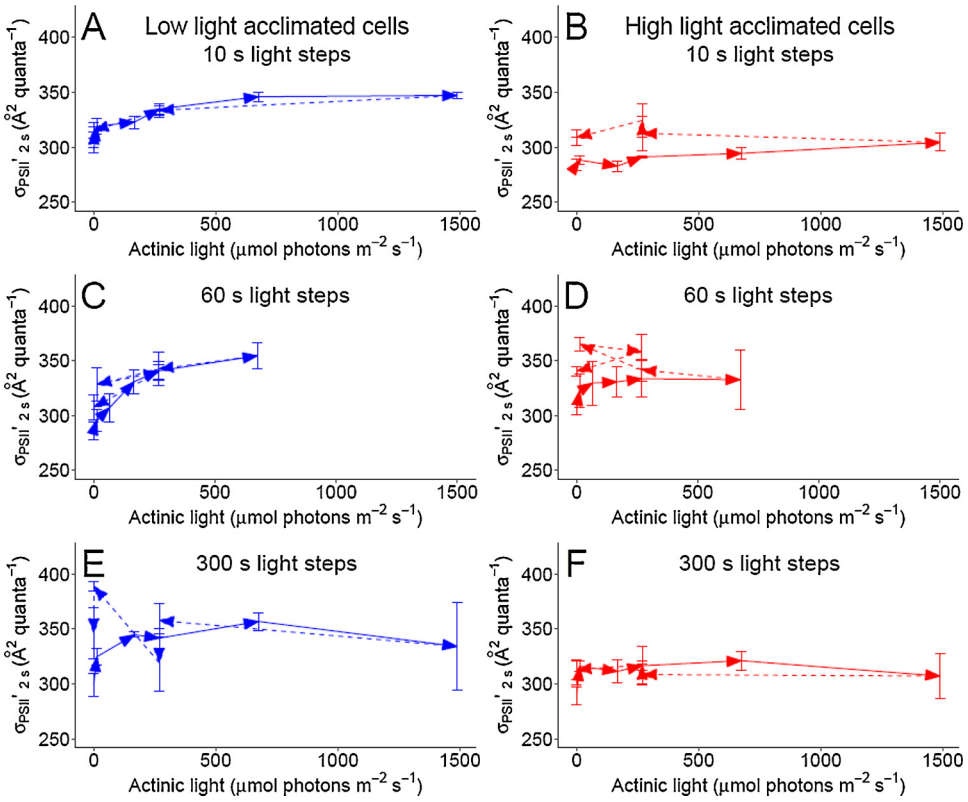

Fig. 4. σ_{PSII} effective absorption cross section for PSII measured after 2 s dark as a function of immediately preceding actinic light level in *C. vulgaris* cultures. Each light period lasted for 10 s (A, B), 60 s (C, D) or 300 s (E, F). Cultures were grown at 30 µmol m^{-2} s^{-1} (low light, A, C, E) or 330 µmol m^{-2} s^{-1} (high light, B, D, F). Arrows show direction of increasing time of treatment. Dashed lines show light steps done after the maximum applied actinic light to emphasize hysteresis of response. Error bars represent standard deviation of three replicates.

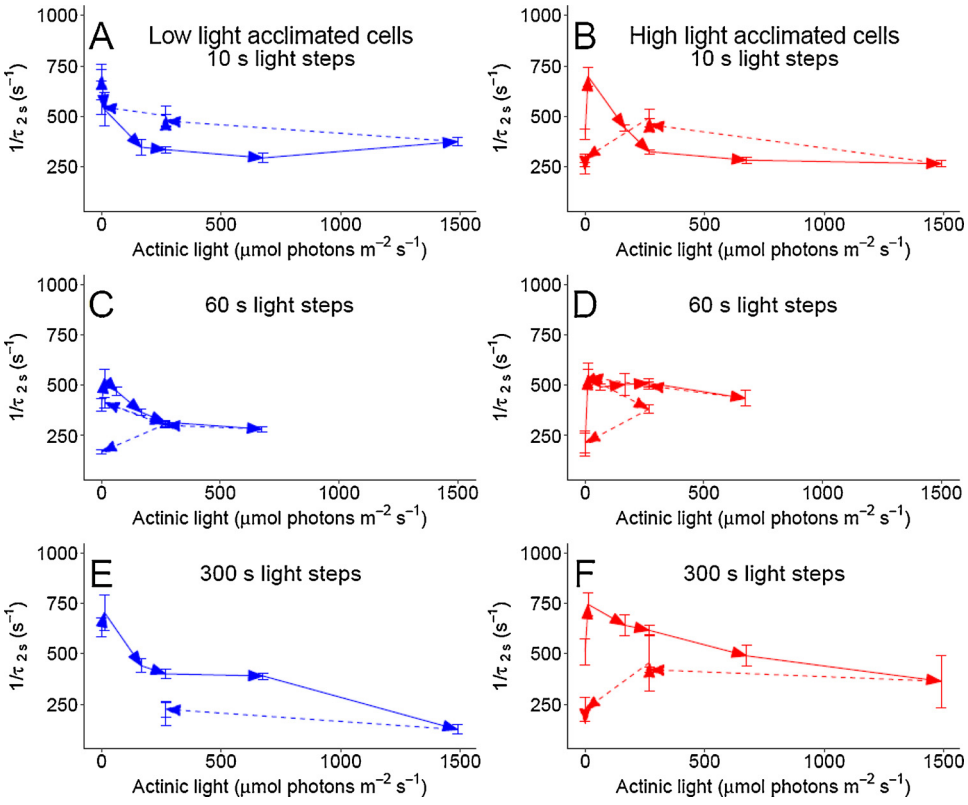

Fig. 5. $1/\tau$ rate constant for re-opening of PSII, measured after 2 s dark as a function of immediately preceding actinic light level in *C. vulgaris* cultures. Each light period lasted for 10 s (A, B), 60 s (C, D) or 300 s (E, F). Cultures were grown at 30 µmol m^{-2} s^{-1} (low light, A, C, E) or 330 µmol m^{-2} s^{-1} (high light, B, D, F). Arrows show direction of increasing time of treatment. Dashed lines show light steps done after the maximum applied actinic light to emphasize hysteresis of response. Error bars represent standard deviation of three replicates.

immediately preceding actinic light level. Now we have our final mechanistic contribution to the accelerations in PSII ETR after transient exposures to super-saturating light (compare Figs. 2A, B with 5 A, B). $1/\tau_{2\,s}$ increases substantially after 10–20 s exposure to supersaturating light. After 60–120 s of exposure to supersaturating light $1/\tau_{2\,s}$ shows scattered responses when cells return to saturating light. But after 300–600 s of exposure to supersaturating light $1/\tau_{2\,s}$ clearly drops when cells return to saturating light. Thus the explanation for the transient acceleration of PSII ETR lies largely in a transient opening of electron sink(s) downstream of PSII, in response to super-saturating

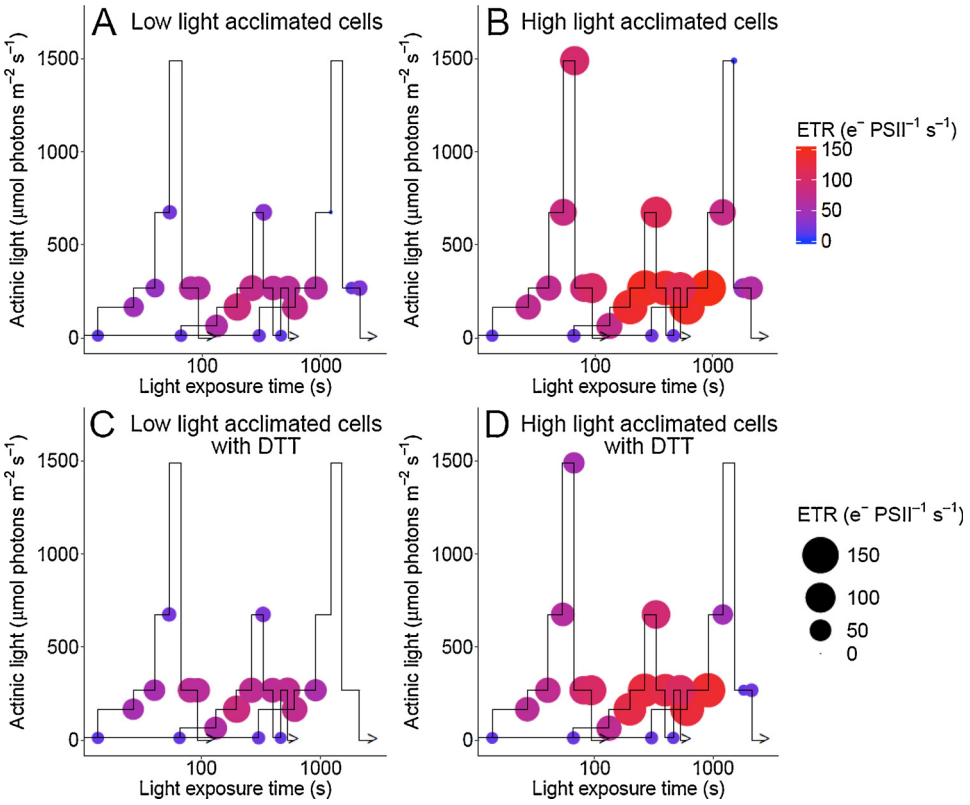

Fig. 6. Actinic light levels (black trace) plotted vs. duration of light exposures PSII ETR (e-PSII^{-1} s^{-1}) in *C. vulgaris* control cultures (A and B) and in presence with DTT (C and D) shown by symbol size and colour scale. Cultures were grown at 30 µmol m^{-2} s^{-1} (Low light, A and C) and 330 µmol m^{-2} s^{-1} (High light, B and D). PSII ETR was estimated according to Eqn. 5.

light.

For *C. vulgaris* grown at both growth limiting (30 µmol m^{-2} s^{-1}) (Fig. 5A, E and C) and growth-saturating (330 µmol m^{-2} s^{-1}) (Fig. 5B, D and F) light, the response patterns of $1/\tau_{2\,s}$ are broadly similar, so the transient opening of electron sink(s) is consistent in cells from both of light acclimations.

To summarize these patterns Fig. 6 shows responses of PSII ETR (e-PSII^{-1} s^{-1}) to actinic light level and duration of light exposure in *C. vulgaris* without and with DTT.

Electron transport rates reach higher maxima in high light acclimated cells (compare Fig. 6A, B). By comparing achieved PSII ETR across equal levels of instantaneous actinic light (Fig. 6A, B) we see strong hystereses in responses, depending upon the previous light history of the sample. In particular the PSII ETR reached its maxima only after short, but not prolonged, prior exposure to super-saturating irradiance. Prolonged exposure to super-saturating irradiance was, in contrast, strongly inhibitory. In cultures incubated with DTT PSII ETR was inhibited under high irradiance, particularly in cultures acclimated to growth at high light (compare Fig. 6B, D).

3.3. PSII inactivation, repair and non-photochemical dissipation

Fig. 7 plots the quantum yield of PSII in the light acclimated state measured after 2 s dark, $F_V'/F_{M'\,2\,s}$ (left Y axes) as a function of time (X axes) with the 300 s period light treatment protocol (grey line, right Y axes) in *C vulgaris* cultures grown at 30 µmol m^{-2} s (low light, A) and at 330 µmol m^{-2} s^{-1} (high light, B).

Across the exposure periods 1–3 at low to moderate light, $F_V'/F_{M'\,2\,s}$ showed modest up regulation from darkness to measures taken under low light (all traces). Upon exposures to super-saturating light periods 4 & 5, $F_V'/F_{M'\,2\,s}$ dropped sharply (all traces), reflecting induction of non-photochemical quenching and/or photoinactivation of PSII. Upon a return to a moderate light for 600 s (periods 6 & 7), $F_V'/F_{M'\,2\,s}$ remained almost steady in the cultures acclimated to low light (Fig. 7A, all traces). It is worth noting that for a same light level, $F_V'/F_{M'\,2\,s}$ was severely inhibited in period 6 as compared to 3. In the cultures grown under high light, $F_V'/F_{M'\,2\,s}$ recovered partially over periods 6 & 7 towards initial levels (Fig. 7B, blue control and red DTT trace). Over the final dark periods 9 & 10, $F_V'/F_{M'\,2\,s}$ remained steady and never reached the initial values (Fig. 7 all traces).

Multiple factors interact to influence the instantaneous $F_V'/F_{M'\,2\,s}$. Sustained forms of NPQs [18,61,62] can keep $F_V'/F_{M'\,2\,s}$ down-regulated even through 2 s of dark relaxation applied to allow photochemical reopening of PSII (Fig. 1). Adding the inhibitor DTT (red trace) to block xanthophyll cycling, which mediates some NPQ mechanisms had little effect upon the observed patterns of down regulation or recovery of $F_V'/F_{M'\,2\,s}$. Thus NPQ responding dynamically through xanthophyll cycle regulation had only a modest influence in cultures acclimated to saturating growth light (Fig. 7B, compare blue control and red DTT traces).

When exposed to high light, PSII can be subject to photoinactivation through multiple mechanisms [63,64], which are countered through a PSII repair cycle [21] which depends upon removal and replacement of PSII subunits dependent on chloroplastic protein degradation and synthesis systems. In cells acclimated to growth-limiting light, inhibition of chloroplast protein synthesis had marginal influences on responses of $F_V'/F_{M'\,2\,s}$ (Fig. 7A, compare blue control and green lincomycin traces). In contrast in cells acclimated to growth-saturating light inhibition of chloroplast protein synthesis accelerated the decline of $F_V'/F_{M'}$ under 600 s of super-saturating light and blocked subsequent partial recovery under 600 s of low light (Fig. 7B, compare blue control and green lincomycin traces). Furthermore as expected for a chlorophyte, the PSII recovery stopped in darkness, because chlorophyte PSII repair depends upon photosynthetic energization [65] in these taxa. Thus, net photoinactivation of PSII function under 300–600 s of supersaturating light contributed to the down-regulation of PSII ETR upon a return to saturating light (Fig. 2C, D). Cells acclimated to growth-saturating light up-regulate their capacity for the repair of PSII photoinactivation and so show stronger responses to loss of PSII repair through lincomycin inhibition.

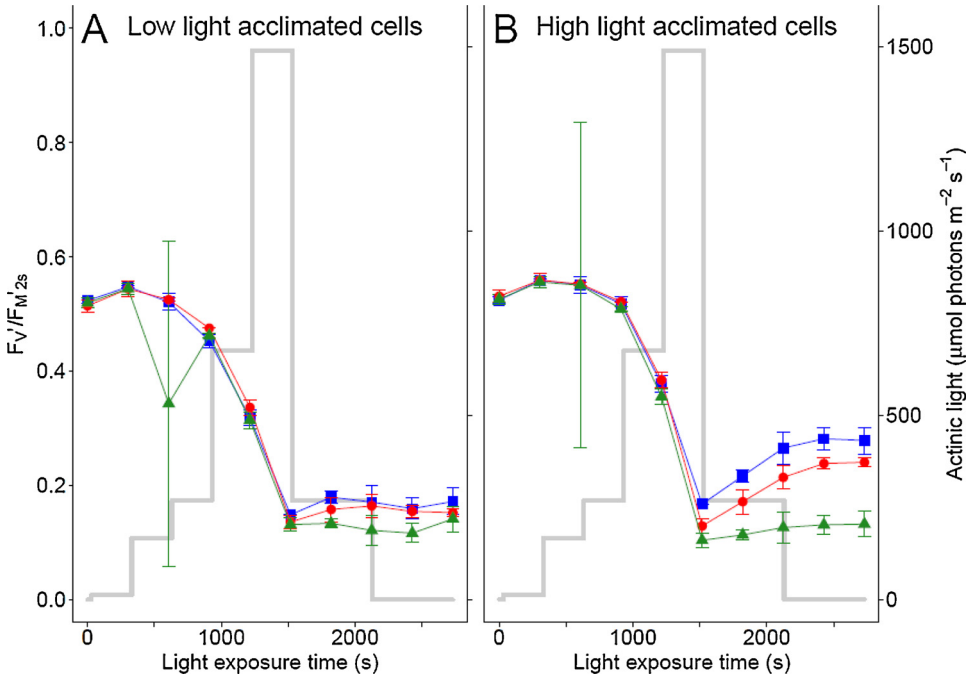

Fig. 7. F_V'/F_M' quantum yield of PSII under light acclimated state for *C. vulgaris* (left Y axes) measured after 2 s dark immediately following the preceding actinic light period (grey trace, right Y axis), plotted vs. elapsed time. Cultures were grown at 30 µmol m^{-2} s^{-1} (A, low Light) or 330 µmol m^{-2} s^{-1} (B, high Light). Blue squares: control cultures. Red circles: cultures with DTT to block the xanthophyll cycle which mediates NPQ. Green triangles: cultures with lincomycin to block PSII repair. Error bars represent standard deviation of three replicates.

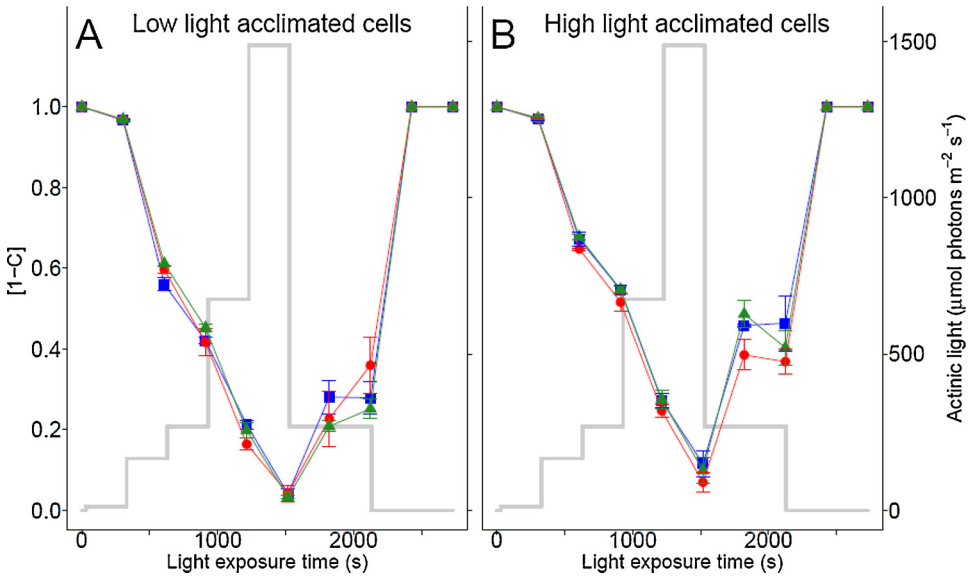

Fig. 8. Fraction of open PSII centres [1-C] for *C. vulgaris* (left Y axes) measured at each actinic light level (grey trace, right Y axis), plotted vs. elapsed time. Cultures grown at 30 µmol m^{-2} s^{-1} (low light, A) or 330 µmol m^{-2} s^{-1} (high light, B). Blue squares: control cultures. Red circles: cultures with DTT to block the xanthophyll cycle. Green triangles: cultures with lincomycin to block PSII repair. Error bars represent standard deviation of three replicates.

The evolution with time of the fraction of open PSII centres ([1-C]) measured in *C. vulgaris* cultures at each actinic light level is shown in Fig. 8. Cells acclimated to low or to high growth light showed similar trajectories of PSII closure in response to changing light, at least at the level of resolution afforded by the changes in irradiance of our protocol. Two independent metrics of PSII closure under excitation ([1-C] and q_P) track each other closely (Supplemental Fig. 1). There is a linear relationship between these two parameters with R^2 equal to 0.9595.

Fig. 9 shows YNPQ for *C. vulgaris* measured at each actinic light level (grey trace, right Y axis), plotted versus time. In cells acclimated to low growth light YNPQ does not accumulate significantly in the shorter light treatment sequence of less than 10 min (Fig. 9A). In contrast the cells acclimated to higher growth light were able to induce significant YNPQ within 10–30 s exposure to moderate light (Fig. 9B). For cells acclimated to either low or high growth light and exposed to longer light treatments (Fig. 9C, D) YNPQ accumulated only after exposure to ~675 µmol photon m^{-2} s^{-1}, sufficient to drive the fraction of open PSII down to ~ 0.2 (Fig. 8). Above that threshold YNPQ induction proceeded at comparable rates in both cultures acclimated to low light or to high light (Fig. 9C, D). Addition of DTT caused a moderate drop in the rate of induction of YNPQ (Fig. 9C, D), while addition of lincomycin to block PSII repair had negligible influence on accumulation of YNPQ (data not shown). This induction of YNPQ corresponded to only marginal down-regulation of σ_{PSII} (Fig. 4E, F), consistent with findings [24] that measured induction of YNPQ does not result in proportional down regulation of σ_{PSII}, but does coincide with the significant down-regulation of YPSII (Fig. 3E, F) and F_V'/F_M' (Fig. 7).

4. Conclusions

Chlorella vulgaris tolerated transient 10–20 s exposures to supersaturating light by transiently accelerating electron transport away from PSII. This mechanism was saturated or overwhelmed by 60–120 s of supersaturating light exposure. With more prolonged exposures induction of YNPQ was induced although in the present work this phenomenon did not significantly down-regulate the effective absorption

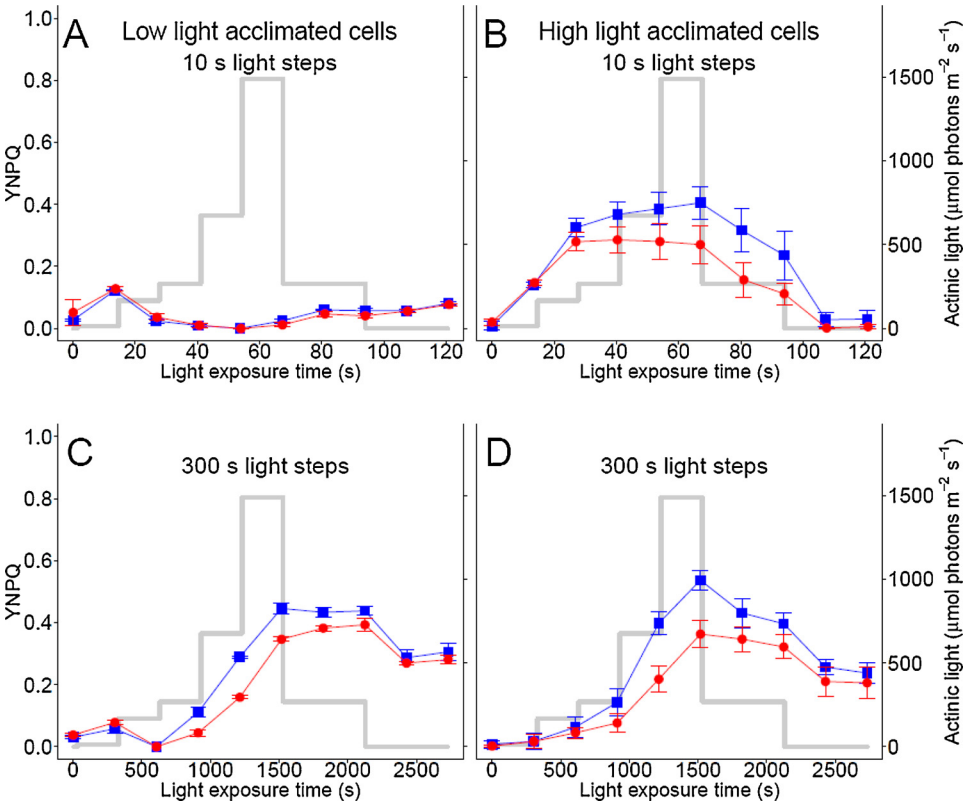

Fig. 9. YNPQ for *C. vulgaris* (left Y axes) measured at each actinic light level (grey trace, right Y axis), plotted vs. elapsed time. Each light period lasted for 10 s (A, B), or 300 s (C, D). Cultures were grown at 30 µmol m^{-2} s^{-1} (low light, A,C) or 330 µmol m^{-2} s^{-1} (high light, B, D). Blue squares: control cultures. Red circles: cultures with DTT to block the xanthophyll cycle. Error bars represent standard deviation of three replicates.

cross section controlling PSII photochemistry efficiency.

Further experiments will aim to translate these results to the conditions encountered in photobioreactors, where the cells undergo significant variations in light, with characteristic times of the order of 10–120 s. Our analysis also demonstrates that kinetic phases of the different mechanisms displayed by the algae to tolerate or exploit fluctuating light are accessible from rapid, non-invasive FRRf measures compatible with online monitoring of photobioreactor performance under mixing and irradiance regimes. This methodology and approach could thus be of great use to control and optimize the phenomenon of light conversion in microalgal solar cultures at large scale.

Authors contributions

Bonnanfant M.: Conception, design and execution of experiments. Collection and assembly of data. Preparation of figures and interpretation of the data. Drafting the article.

Jesus B.: Analysis and interpretation of the data. Critical revision of the article.

Pruvost J.: Provision of study material. Conception of experiments. Critical revision of the article.

Mouget J.L.: Obtaining funding. Critical revision of the article.

Campbell D.A.: Conception and design of experiments. Technical support. Collection and assembly of the data. Analysis and interpretation of the data. Drafting and revision of the article.

Declaration of Competing Interest

Authors declare there is no potential financial or other interests that could be perceived to influence the outcomes of the research.

Acknowledgements

This publication was supported by the European Commission under the Horizon 2020 Research and Innovation Program GHaNA (the Genus Haslea, New marine resources for blue biotechnology and Aquaculture) under Grant Agreement No 734708/GHANA/H2020-MSCA-RISE-2016 (JLM); the Pays de la Loire region programme AMI (Atlantic MIcroalgae); The Canada Research Chairs (DC) and by the European Researcher Mobility Program of the Czech Academy of Sciences (CZ.02.2.69/0.0/0.0/16_027/0007990). Equipment used in the study was funded by the New Brunswick Innovation Foundation, the Canada Foundation for Innovation, and the Natural Sciences and Engineering Research Council of Canada (DC).

The authors thank Miranda Corkum for assistance with microbial culturing.

Appendix A. Supplementary data

Supplementary material related to this article can be found, in the online version, at doi:https://doi.org/10.1016/j.algal.2019.101713.

References

[1] A. Richmond, Handbook of Microalgal Culture: Biotechnology and Applied Phycology, John Wiley & Sons, 2008.
[2] F. Le Borgne, Développement d'un photobioréacteur solaire intensifié en vue de la production à grande échelle de biomasse microalgale, thesis, Nantes, (2011) (Accessed January 23, 2019), http://www.theses.fr/2011NANT2025.
[3] J.A. Duffie, W.A. Beckman, Solar Engineering of Thermal Processes, (2013), p. 928.
[4] J. Pruvost, J.-F. Cornet, J. Legrand, Hydrodynamics influence on light conversion in photobioreactors: an energetically consistent analysis, Chem. Eng. Sci. 63 (2008) 3679–3694, https://doi.org/10.1016/j.ces.2008.04.026.
[5] M. Janssen, P. Slenders, J. Tramper, L.R. Mur, RenéH. Wijffels, Photosynthetic efficiency of Dunaliella tertiolecta under short light/dark cycles, Enzyme Microb. Technol. 29 (2001) 298–305, https://doi.org/10.1016/S0141-0229(01)00387-8.
[6] C. Vejrazka, M. Janssen, M. Streefland, R.H. Wijffels, Photosynthetic efficiency of Chlamydomonas reinhardtii in flashing light, Biotechnol. Bioeng. 108 (2011) 2905–2913, https://doi.org/10.1002/bit.23270.
[7] H. Takache, J. Pruvost, H. Marec, Investigation of light/dark cycles effects on the photosynthetic growth of Chlamydomonas reinhardtii in conditions representative of photobioreactor cultivation, Algal Res. 8 (2015) 192–204, https://doi.org/10.1016/j.algal.2015.02.009.
[8] P.J. Graham, B. Nguyen, T. Burdyny, D. Sinton, A penalty on photosynthetic growth in fluctuating light, Sci. Rep. 7 (2017) 12513, https://doi.org/10.1038/s41598-017-12923-1.

[9] A. Kazbar, Etude de l'impact de la concentration en oxygène dissous et la présence d'une fraction sombre sur la performance des photobioréacteurs, thesis, Nantes, (2018) (Accessed January 24, 2019), http://www.theses.fr/2018NANT4007.

[10] A.R. Crofts, C.A. Wraight, The electrochemical domain of photosynthesis, Biochim. Biophys. Acta BBA - Rev. Bioenergy 726 (1983) 149–185, https://doi.org/10.1016/0304-4173(83)90004-6.

[11] A. Sukenik, J. Bennett, P. Falkowski, Light-saturated photosynthesis — Limitation by electron transport or carbon fixation? Biochim. Biophys. Acta BBA - Bioenerg. 891 (1987) 205–215, https://doi.org/10.1016/0005-2728(87)90216-7.

[12] Z. Kolber, P.G. Falkowski, Use of active fluorescence to estimate phytoplankton photosynthesis in situ, Limnol. Oceanogr. 38 (1993) 1646–1665, https://doi.org/10.4319/lo.1993.38.8.1646.

[13] O. Prasil, Z. Kolber, J.A. Berry, P.G. Falkowski, Cyclic electron flow around Photosystem II in vivo, Photosynth. Res. 48 (1996) 395–410, https://doi.org/10.1007/BF00029472.

[14] K. Asada, The water-water cycle as alternative photon and electron sinks, Philos. Trans. R. Soc. B Biol. Sci. 355 (2000) 1419–1431.

[15] K.C. Valle, M. Nymark, I. Aamot, K. Hancke, P. Winge, K. Andresen, G. Johnsen, T. Brembu, A.M. Bones, System responses to equal doses of photosynthetically usable radiation of blue, green, and red light in the marine diatom Phaeodactylum tricornutum, PLoS One 9 (2014) e114211, , https://doi.org/10.1371/journal.pone.0114211.

[16] J.F. Allen, State transitions–a question of balance, Science 299 (2003) 1530–1532, https://doi.org/10.1126/science.1082833.

[17] J. Kargul, J. Barber, Photosynthetic acclimation: structural reorganisation of light harvesting antenna – role of redox-dependent phosphorylation of major and minor chlorophyll *a*/*b* binding proteins, FEBS J. 275 (2008) 1056–1068, https://doi.org/10.1111/j.1742-4658.2008.06262.x.

[18] R. Goss, B. Lepetit, Biodiversity of NPQ, J. Plant Physiol. 172 (2015) 13–32, https://doi.org/10.1016/j.jplph.2014.03.004.

[19] Z. Dubinsky, N. Stambler, Photoacclimation processes in phytoplankton: mechanisms, consequences, and applications, Aquat. Microb. Ecol. 56 (2009) 163–176, https://doi.org/10.3354/ame01345.

[20] B. Kok, Photosynthesis in flashing light, Biochim. Biophys. Acta 21 (1956) 245–258, https://doi.org/10.1016/0006-3002(56)90004-X.

[21] P.J. Nixon, F. Michoux, J. Yu, M. Boehm, J. Komenda, Recent advances in understanding the assembly and repair of photosystem II, Ann. Bot. 106 (2010) 1–16, https://doi.org/10.1093/aob/mcq059.

[22] Y. Huot, M. Babin, Overview of fluorescence protocols: theory, basic concepts, and practice, in: D.J. Suggett, O. Prášil, M.A. Borowitzka (Eds.), Chlorophyll Fluoresc. Aquat. Sci. Methods Appl. Springer, Netherlands, 2010, pp. 31–74.

[23] Z.S. Kolber, O. Prášil, P.G. Falkowski, Measurements of variable chlorophyll fluorescence using fast repetition rate techniques: defining methodology and experimental protocols, Biochim. Biophys. Acta BBA - Bioenergy 1367 (1998) 88–106.

[24] K. Xu, J. Lavaud, R. Perkins, E. Austen, M. Bonnanfant, D.A. Campbell, Phytoplankton σPSII and excitation dissipation; implications for estimates of primary productivity, Front. Mar. Sci. 5 (2018).

[25] B. Lepetit, G. Gélin, M. Lepetit, S. Sturm, S. Vugrinec, A. Rogato, P.G. Kroth, A. Falciatore, J. Lavaud, The diatom *Phaeodactylum tricornutum* adjusts non-photochemical fluorescence quenching capacity in response to dynamic light via fine-tuned Lhcx and xanthophyll cycle pigment synthesis, New Phytol. (2016).

[26] K.H. Halsey, B.M. Jones, Phytoplankton strategies for photosynthetic energy allocation, Annu. Rev. Mar. Sci. 7 (2015) 265–297.

[27] K.H. Halsey, A.J. Milligan, M.J. Behrenfeld, Physiological optimization underlies growth rate-independent chlorophyll-specific gross and net primary production, Photosynth. Res. 103 (2010) 125–137, https://doi.org/10.1007/s111. doi: 2 0-009-95. doi: 2 6-z.

[28] K. Felcmanová, M. Lukeš, E. Kotabová, E. Lawrenz, K.H. Halsey, O. Prášil, Carbon use efficiencies and allocation strategies in Prochlorococcus marinus strain PCC 9511 during nitrogen-limited growth, Photosynth. Res. 134 (2017) 71–82, https://doi.org/10.1007/s11120-017-0418-3.

[29] R. Perkins, C. Williamson, J. Lavaud, J.-L. Mouget, D.A. Campbell, Time-dependent upregulation of electron transport with concomitant induction of regulated excitation dissipation in Haslea diatoms, Photosynth. Res. (2018), https://doi.org/10.1007/s111. doi: 2 0-018-0508-x.

[30] P.G. Falkowski, T.G. Owens, Light–Shade adaptation 1, Plant Physiol. 66 (1980) 592–595.

[31] R.G. Perkins, J.-L. Mouget, S. Lefebvre, J. Lavaud, Light response curve methodology and possible implications in the application of chlorophyll fluorescence to benthic diatoms, Mar. Biol. 149 (2006) 703–712, https://doi.org/10.1007/s00227-005-0222-z.

[32] M.W. Beyerinck, Culturversuche mit Zoochlorellen, Lichenengonidien und anderen niederen Algen, (1890).

[33] J.R.F. Malapascua, C.G. Jerez, M. Sergejevová, F.L. Figueroa, J. Masojídek, Photosynthesis monitoring to optimize growth of microalgal mass cultures: application of chlorophyll fluorescence techniques, Aquat. Biol. 22 (2014) 123–140, https://doi.org/10.3354/ab00597.

[34] J. Serôdio, W. Schmidt, S. Frankenbach, A chlorophyll fluorescence-based method for the integrated characterization of the photophysiological response to light stress, J. Exp. Bot. 68 (2017) 1123–1135, https://doi.org/10.1093/jxb/erw49. doi: 2.

[35] A. Richmond, Handbook of Microalgal Culture: Biotechnology and Applied Phycology, John Wiley & Sons, 2008.

[36] G. Ni, G. Zimbalatti, C.D. Murphy, A.B. Barnett, C.M. Arsenault, G. Li, A.M. Cockshutt, D.A. Campbell, Arctic Micromonas uses protein pools and non-photochemical quenching to cope with temperature restrictions on Photosystem II protein turnover, Photosynth. Res. (2016), https://doi.org/10.1007/s111. doi: 2 0-016-0310-6.

[37] W. Bilger, O. Björkman, Role of the xanthophyll cycle in photoprotection elucidated by measurements of light-induced absorbance changes, fluorescence and photosynthesis in leaves of Hedera canariensis, Photosynth. Res. 25 (1990) 173–185, https://doi.org/10.1007/BF00033159.

[38] C. Six, Z. Finkel, A. Irwin, D. Campbell, Light variability illuminates niche-partitioning among marine picocyanobacteria, PLoS One (2007).

[39] K.M. Bachmann, V. Ebbert, W.W. Adams III, A.S. Verhoeven, B.A. Logan, B. Demmig-Adams, Effects of lincomycin on PSII efficiency, non-photochemical quenching, D1 protein and xanthophyll cycle during photoinhibition and recovery, Funct. Plant Biol. 31 (2004) 803–813, https://doi.org/10.1071/FP04022 (accessed January 27, 2014).

[40] S.R. Laney, Assessing the error in photosynthetic properties determined with Fast Repetition Rate fluorometry, Limnol. Oceanogr. 48 (2003) 2234–2242.

[41] R. Perkins, C. Williamson, J. Lavaud, J.-L. Mouget, D.A. Campbell, Time-dependent upregulation of electron transport with concomitant induction of regulated excitation dissipation in Haslea diatoms, Photosynth. Res. 137 (2018) 377–388, https://doi.org/10.1007/s111. doi: 2 0-018-0508-x.

[42] B. Jesus, A. Ciochetti, D.A. Campbell, C. Williamson, psifluo, (2018).

[43] R Core Team, R: A Language and Environment for Statistical Computing, R Foundation for Statistical Computing, Vienna, Austria, 2017https://www.R-project.org/.

[44] J. Cao, Govindjee, Chlorophyll *a* fluorescence transient as an indicator of active and inactive photosystem II in thylakoid membranes, Biochim. Biophys. Acta BBA - Bioenergy 1015 (1990) 180–188, https://doi.org/10.1016/0005-. doi: 2 7. doi: 2 8(90)90018-Y.

[45] B. Genty, J.-M. Briantais, N.R. Baker, The relationship between the quantum yield of photosynthetic electron transport and quenching of chlorophyll fluorescence, Biochim. Biophys. Acta BBA - Gen. Subj. 990 (1989) 87–92, https://doi.org/10.1016/S0304-4165(89)80016-9.

[46] C. Klughammer, U. Schreiber, Complementary PS II quantum yields calculated from simple fluorescence parameters measured by PAM fluorometry and the Saturation Pulse method, PAM Appl. Notes. 1 (2008) 27–35.

[47] J. Serôdio, S. Cruz, S. Vieira, V. Brotas, Non-photochemical quenching of chlorophyll fluorescence and operation of the xanthophyll cycle in estuarine microphytobenthos, J. Exp. Mar. Biol. Ecol. 326 (2005) 157–169, https://doi.org/10.1016/j.jembe.. doi: 2 005.05.011.

[48] D. Suggett, H. MacIntyre, T. Kana, R. Geider, Comparing electron transport with gas exchange: parameterising exchange rates between alternative photosynthetic currencies for eukaryotic phytoplankton, Aquat. Microb. Ecol. 56 (2009) 147–162, https://doi.org/10.3354/ame01303.

[49] D.M. Kramer, G. Johnson, O. Kiirats, G.E. Edwards, New fluorescence parameters for the determination of Q_A redox state and excitation energy fluxes, Photosynth. Res. 79 (2004) 209–218, https://doi.org/10.1023/B:PRES.0000015391.99477.0d.

[50] D.J. Hughes, D.A. Campbell, M.A. Doblin, J.C. Kromkamp, E. Lawrenz, C.M. Moore, K. Oxborough, O. Prášil, P.J. Ralph, M.F. Alvarez, D.J. Suggett, Roadmaps and Detours: Active Chlorophyll- a Assessments of Primary Productivity Across Marine and Freshwater Systems, Environ. Sci. Technol. (2018), https://doi.org/10.1021/acs.est.8b03488.

[51] D. Suggett, H. MacIntyre, T. Kana, R. Geider, Comparing electron transport with gas exchange: parameterising exchange rates between alternative photosynthetic currencies for eukaryotic phytoplankton, Aquat. Microb. Ecol. 56 (2009) 147–162, https://doi.org/10.3354/ame01303.

[52] R Studio Team, RStudio: Integrated Development Environment for R, RStudio, Inc., Boston, MA, 2018http://www.rstudio.com/.

[53] Elzhov, minpack.lm: R Interface to the Levenberg-Marquardt Nonlinear Least-Squares Algorithm Found in MINPACK, Plus Support for Bounds, n.d.

[54] W.N. Venables, B.D. Ripley, Modern Applied Statistics with S, Springer, 2002, http://www.stats.ox.ac.uk/pub/MASS4.

[55] Baty Florent, Ritz Christian, Charles Sandrine, Brutsche Martin, Flandrois Jean-Pierre, Delignette-Muller Marie-Laure, A toolbox for nonlinear regression in r: the package nlstools, J. Stat. Softw. 66 (2015) 1–21 http://www.jstatsoft.org/v66/i05/.

[56] Wickham Hadley, ggplot2: Elegant Graphics for Data Analysis, Springer-Verl, N. Y, 2009http://ggplot2.org.

[57] Wickham Hadley, tidyverse: Easily Install and Load "Tidyverse" Packages, (2017) https://CRAN.R-project.org/package=tidyverse.

[58] Kassambara Alboukadel, ggpubr: "ggplot2" Based Publication Ready Plots, (2017) https://CRAN.R-project.org/package=ggpubr.

[59] Auguie Baptiste, gridExtra: Miscellaneous Functions for "Grid" Graphics, (2017) https://CRAN.R-project.org/package=gridExtra.

[60] Soetaert Karline, shape: Functions for Plotting Graphical Shapes, Colors, (2018) https://CRAN.R-project.org/package=shape.

[61] H. Wu, A.M. Cockshutt, A. McCarthy, D.A. Campbell, Distinctive photosystem II photoinactivation and protein dynamics in marine diatoms, Plant Physiol. 156 (2011) 2184–2195, https://doi.org/10.1104/pp.111.17877.

[62] J. Lavaud, B. Lepetit, An explanation for the inter-species variability of the photoprotective non-photochemical chlorophyll fluorescence quenching in diatoms, Biochim. Biophys. Acta BBA – Bioenergy 1827 (2013) 294–302, https://doi.org/10.1016/j.bbabio.2012.11.012.

[63] C.D. Murphy, M.S. Roodvoets, E.J. Austen, A. Dolan, A. Barnett, D.A. Campbell, Photoinactivation of photosystem II in Prochlorococcus and Synechococcus, PLoS One 12 (2017) e0168991, , https://doi.org/10.1371/journal.pone.0168991.

[64] R. Oguchi, I. Terashima, J. Kou, W.S. Chow, Operation of dual mechanisms that both lead to photoinactivation of Photosystem II in leaves by visible light, Physiol. Plant. 142 (2011) 47–55, https://doi.org/10.1111/j.1399-3054.2011.01452.x.

[65] M. Edelman Marvin, D1-protein dynamics in photosystem II: the lingering enigma, Photosynth. Res. 98 (2008) 609–620.